

EVOLUTION OF BCGS STRUCTURAL PARAMETERS IN THE LAST ~ 6 GYR: FEEDBACK PROCESSES VERSUS MERGER EVENTS.

B. ASCASO¹

¹ Department of Physics, University of California, Davis, One Shields Avenue, Davis, CA 95616, USA

J. A. L. AGUERRI^{2,3}, J. VARELA, A. CAVA^{2,3}

² Instituto de Astrofísica de Canarias, C/ Vía Láctea s/n, 38200 La Laguna, Tenerife, Spain

³ Departamento de Astrofísica, Universidad de La Laguna E-38205, La Laguna, Tenerife, Spain

D. BETTONI⁴

⁴ INAF- Osservatorio Astronomico di Padova, Vicolo Osservatorio 5, 35122, Padova, Italy

M. MOLES^{5,6}

⁵ Instituto de Astrofísica de Andalucía-CSIC, Glorieta de la Astronomía s/n, 18008, Granada, Spain

⁶ Centro de Estudios de Física del Cosmos de Aragón(CEFCA), C/General Pizarro 1, 44001, Teruel, Spain

M. D'ONOFRIO⁷

⁷ Dip. Astronomia, Università di Padova, Vicolo Osservatorio 2, 35122 Padova, Italy

Draft version May 15, 2022

ABSTRACT

We present results on the evolution in the last 6 Gyr of the structural parameters of two samples of brightest cluster galaxies (BCGs). The nearby sample of BCGs consist on 69 galaxies from the WINGS survey spanning a redshift range of $0.04 < z < 0.07$. The intermediate redshift ($0.3 < z < 0.6$) sample is formed by 20 BCGs extracted from the Hubble Space Telescope archive. Both samples have similar spatial resolution and their host clusters have similar X-ray luminosities. We report an increase in the size of the BCGs from intermediate to local redshift. However, we do not detect any variation in the Sérsic shape parameter in both samples. These results are proved to be robust since the observed tendencies are model independent. We also obtain significant correlations between some of the BCGs parameters and the main properties of the host clusters. More luminous, larger and centrally located BCGs are located in more massive and dominant galaxy clusters. These facts indicate that the host galaxy cluster has played an important role in the formation of their BCGs. We discuss the possible mechanisms that can explain the observed evolution of the structural parameters of the BCGs. We conclude that the main mechanisms that can explain the increase in size and the non-evolution in the Sérsic shape parameter of the BCGs in the last 6 Gyr are feedback processes. This result disagrees with semi-analytical simulation results supporting that merging processes are the main responsible for the evolution of the BCGs until the present epoch.

Subject headings: galaxies: clusters – galaxies:general – galaxies: elliptical and lenticular, cD – galaxies: evolution – galaxies: formation – galaxies: fundamental parameters

1. INTRODUCTION

The Brightest Cluster Galaxies (BCGs) are the most luminous and massive stellar systems in the Universe. BCGs are usually found very close to the center of the clusters of galaxies determined from X-ray or gravitational lensing observations (Jones & Forman 1984; Smith et al. 2005). This suggests that the brightest cluster members have settled down in the potential well of the cluster (but see also Coziol et al. 2009). These special objects possess a number of singular properties, being their origin and evolution directly related with the mass assembly in galaxy clusters.

BCGs luminosities are remarkably homogenous, as noticed first by Humason, Mayall & Sandage (1956). A number of works (Sandage 1972a; Gunn & Oke 1975; Hoessel & Schneider 1985; Postman & Lauer 1995), ver-

ified their high luminosities and small scatter in absolute magnitude and consequently, proposed them as *standard candles* for measuring cosmological distances. In fact, they were originally used to increase the range of Hubble's redshift - distance law (Sandage 1972a,b).

Furthermore, there are numerous pieces of evidence showing that BCGs are not extracted from the same luminosity distribution function as normal galaxies (Tremaine & Richstone 1977; Loh & Strauss 2006; Ascaso et al. 2008; Ascaso 2008; Lin et al. 2009). Those differences could be related with the formation of BCGs in a different way than normal elliptical galaxies. There are indications that the environment plays an important role in the formation of BCGs due to their special location in the cluster. Thus, several works found correlations between the BCGs luminosity and the mass

or the X-ray luminosity of the clusters (Brough et al. 2002; Nelson et al. 2002; Lin & Mohr 2004; Whiley et al. 2008; Sanderson et al. 2009). Lambas et al. (1988) even discovered an alignment between the major axis of the BCGs and the distribution of galaxies around the clusters located in 15 Mpc scales.

On a different perspective, considerable observational evidence (Bower, Lucey & Ellis 1992a; Arag3n-Salamanca et al. 1993; Stanford, Eisenhardt & Dickinson 1998; van Dokkum et al. 1998; Miley et al. 2006; van Dokkum et al. 2010) suggest that the stars of giant elliptical galaxies were formed at high redshift, and have been passively evolving to the present day, but see also Mancini et al. (2010). Nevertheless, this passive evolution is different from normal elliptical galaxies because stellar population studies show that BCGs are more metallic and have larger α -enhancement than normal elliptical galaxies (Loubser et al. 2009). This passive evolution of the stellar population is in apparent contradiction with some studies showing an evolution of the size and mass of BCGs. For instance, Arag3n-Salamanca et al. (1998) found that BCG galaxies have grown their masses in the last 8 Gyr. Nelson et al. (2002) reported a growth of ~ 2 at $z \sim 0.5$ and Bernardi (2009) showed that BCGs at $z \sim 0.25$ are 70% smaller in size than nearby ones.

On the other hand, the surface brightness profiles of BCGs are usually well fitted by de Vaucouleurs or S3rsic profiles even at large radii (Graham et al. 1996), similar to normal elliptical galaxies (Trujillo et al. 2001; Graham & Guzm3n 2003; Aguerri et al. 2004; Kormendy et al. 2009). Nevertheless, some of them show an excess of light, usually called envelopes, over the $r^{1/4}$ profile at large radii (Matthews, Morgan & Schmidt 1964; Oemler 1973, 1976; Schombert 1986, 1987, 1988; Gonzalez et al. 2005; Seigar, Graham & Jerjen 2007). These envelopes show low surface brightness and large spatial extension (Zibetti et al. 2005). Although the origin of such extended envelopes is still not completely clear, Patel et al. (2006) claimed that the extended stellar haloes of the BCGs are likely from the BCGs themselves (see also the works on M87; Arnaboldi et al. 2004; Doherty et al. 2009). These extended stellar haloes are not part of the so-called intracluster light (ICL) formed by non-bounded stars and observed in some nearby clusters (Arnaboldi et al. 2002; Aguerri et al. 2005a; Gerhard et al. 2007; Castro-Rodr3guez et al. 2009). They are formed by stars gravitationally bounded to the BCG. Nevertheless, the origin of the extended envelopes could be related to the origin of the ICL (e.g. Murante et al. 2007).

Different theories have been proposed to explain the observational properties of BCGs and give a framework about their formation. BCGs were proposed to be formed by the accumulation of tidal stripped debris from clusters of galaxies (Ostriker & Tremaine 1975; McGlynn & Ostriker 1980; Merritt 1985). Galaxy cannibalism in the central regions of galaxy clusters can also produce massive galaxies similar to BCGs (Ostriker & Hausman 1977). Also, Fabian, Nulsen & Canizares (1982) proposed gas cooling flows presented in the centers of galaxy clusters as the

responsible for creating these systems.

During the last decade the cold dark matter (CDM) scenario has been considered the most appropriate in order to explain the structure formation in the Universe. This galaxy formation scenario can also explain the formation of BCGs. Thus, Dubinski (1998) showed that natural merging process of dark matter haloes in a hierarchical model can produce central galaxies with similar surface brightness and velocity dispersion as the observed ones. Recently, hierarchical simulations of structure formation have shown that the stellar component of BCGs was formed at early epochs (50% at $z \sim 5$ and 80% at $z \sim 3$) in separated galaxies which then, accreted material to form the BCG through dry mergers (De Lucia & Blaizot 2007). This implies that most of the stars located actually in BCGs were not formed in situ. In contrast, they were accreted from galaxy satellites over the formation history of the galaxy. These accreted stars built up the extended haloes observed on BCGs (Abadi et al. 2006; Murante et al. 2007). Recently, it was found that the period of mass growth of BCGs is shorter than the expected from numerical simulations (Collins et al. 2009).

In this paper, we have explored the properties of a sample of nearby BCGs from WINGS (Wide-field Nearby Galaxy-cluster Survey, Fasano et al. 2006). We have analyzed their surface brightness distribution, and performed a study of their structural parameters and morphology. We have studied the evolution of all those properties by comparing them with a higher redshift BCGs sample ($0.3 < z < 0.6$) imaged with the Advanced Camera for Surveys (ACS) at the Hubble Space Telescope (HST). Additionally, we have also compared the structural parameters that define the BCGs with the global parameters of the host clusters. This dataset allows to investigate the evolution of the structural parameters of BCGs in a period of ~ 6 Gyr and give valuable indications about the mass assembly in galaxy clusters.

The structure of this paper is as follows. In Section 2, we present the BCGs samples we have analyzed in this paper. In Section 3, we analyze and explain the procedures used for fitting the galaxies surface brightness. In Section 4, we show the evolution with redshift of the BCGs structural parameters, magnitudes and envelope light. Section 5 is devoted to the search for relations between the BCGs and their host cluster properties. Finally, we show the discussion and conclusions of this work in Section 6 respectively. Throughout this paper we have adopted the same WINGS Λ CDM cosmology: $H_0 = 70 \text{ km s}^{-1} \text{ Mpc}^{-1}$, $\Omega_m = 0.3$ and $\Omega_\Lambda = 0.7$.

2. DATA SAMPLE

In this work, we have analyzed the population of BCGs in two samples. On one hand, we have selected the BCGs in WINGS (Fasano et al. 2006). This cluster survey consist on 77 clusters in the redshift range of $0.04 \leq z \leq 0.07$, 36 of them were observed from the North hemisphere with the Wide Field Camera (WFC) mounted at the Isaac Newton Telescope (INT)-2.5m at La Palma, Spain, while the remaining 41 ones were imaged with the Wide Field Imager (WFI) in Max Planck Gesellschaft (MPG-ESO)-2.2m in La Silla, Chile. All clusters were imaged throughout the V band pass. The images were taken under seeing conditions of $\sim 1''$, implying that the typical resolution for these images was $\sim 1 \text{ kpc}$.

The WINGS clusters were selected from the X-ray ROSAT catalogues (Ebeling et al. 1996) with X-ray fluxes $\geq 5.0 \times 10^{-12} \text{ erg cm}^{-2} \text{ s}^{-1}$ in the 0.1-2.4 keV band and $|b| > 20$ deg. This survey has a compromise to obtain a large spatial coverage (around 1.6-2.7 Mpc radius) and depth (complete up to $V \sim 21.7$ mag at 90%, Varela et al. 2009). The analysis of the properties of such clusters can help to determine a zero point comparison in the properties of local clusters with respect to higher redshift surveys. The main properties of the BCGs in WINGS sample are listed in Table 1 in Fasano et al. (2010).

We have excluded eight BCGs from this sample due to different issues. A193 has three galaxies interacting with the BCG. RXJ0058 and A2626 consist on a couple of galaxies with probably an AGN in one of them. In addition, the BCGs in A133, A160, A780, A3164 and IIZW108 are either too close to the edge of the chip or have closer stars. These facts make our fit not to converge to a good solution. Then, the final sample consists on 69 BCGs.

On the other hand, we have selected an intermediate redshift sample of 20 BCGs ($0.3 < z < 0.6$) extracted from the HST archive. These BCGs belong to a cluster sample observed with the Advanced Camera for Surveys (ACS) in the Hubble Space Telescope (HST) through the F814W band, spanning the same range of X-ray luminosity than WINGS. The high resolution of the ACS makes that the minimum scale that we can resolve in the intermediate redshift clusters is similar (~ 0.6 kpc) to the typical resolution in the WINGS sample.

The ACS observations were carried out in Cycle 13 and 14 (proposals 10490 and 10152). The BCGs were observed in single pointings of more than 2000 seconds. The original sample consisted of a complete, homogeneous sample of 72 X-ray clusters (Mullis et al. 2003). From this sample, 26 were observed with the snapshot program. We just selected the BCGs that were clearly the brightest from the cluster and had spectroscopic or photometric redshift available from the NED database. The final sample consists on 20 BCGs.

The galaxy clusters in the ACS sample were observed through a different band-pass than nearby clusters. In order to have the same rest-frame magnitudes for nearby and intermediate redshift galaxies, we have transformed the F814W-band to V-band rest-frame using the following transformation:

$$V(0) - F814W(z) = (V - F814W)_0 - k_{F814W} - EC_{F814W} \quad (1)$$

where k_{F814W} and EC_{F814W} are the K-correction and evolutionary correction in the F814W band (Poggianti 1997), and $(V - F814W)_0$ is the rest-frame (V-F814W) color. The surface brightness of the galaxies was also corrected from cosmological dimming.

The top panel in Figure 1 shows the X-ray luminosity distribution for the ACS clusters sample, with the X-ray distribution function of the whole WINGS sample overplotted. The bottom panel in the same Figure refers to the cumulative function of the ACS clusters sample. We have also overplotted here the accumulated function of those WINGS clusters showing the same range of X-ray luminosity as the ACS sample, $5 \times 10^{43} < L_x < 2.52 \times 10^{44} \text{ erg s}^{-1}$. We have performed

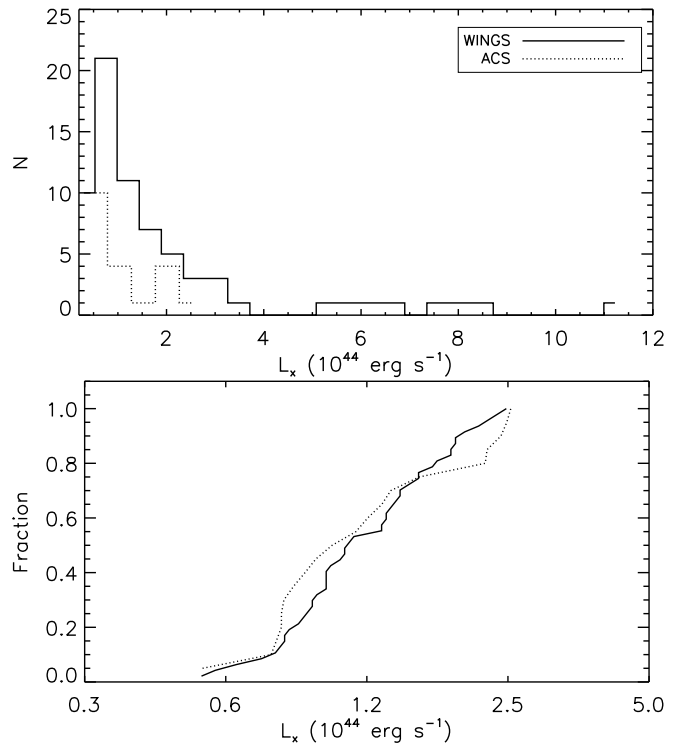


FIG. 1.— L_x distribution of the clusters sample in WINGS (solid line) and ACS (dotted line). The top panel shows the overall distribution for the whole ACS and WINGS sample, while the bottom panel refers to the cumulative distribution for the ACS sample and the WINGS X-ray luminosity restricted sample.

a Kolmogorov-Smirnoff (KS) test in these two samples, resulting that both distributions are statistically similar. This implies that the global cluster properties (i.e. mass, velocity dispersion) are similar in the selected nearby and intermediate redshift galaxy cluster samples. The cluster mass evolution has non effect in this selection since we have previously checked that there is not trend between L_x of the host cluster and the BCG effective radius in both samples. In Tables 1 and 2, we list the names of the BCGs in the WINGS and ACS sample respectively, together with their coordinates, X-ray luminosity and redshift of the host cluster.

3. SURFACE BRIGHTNESS ANALYSIS

We analyzed the surface brightness distribution of the galaxies by using GASP2D (Méndez-Abreu et al. 2008; Ascaso et al. 2009). This routine fits the 2D surface brightness distribution of galaxies with one or two components following a particular surface brightness model. In particular, we have fit the surface brightness of the galaxies with two components: Sérsic (Sérsic 1968) and exponential (Sérsic 1968; Freeman 1970).

All the information regarding GASP2D can be found in Méndez-Abreu et al. (2008). Here, we will only mention some important remarks. GASP2D fits individually each galaxy. It first masks the rest of the galaxies in the frame automatically. After that, the user is allowed to modify them in case some galaxies have not been correctly deblended or detected.

GASP2D adopts a Levenberg-Marquardt algorithm to fit the two-dimensional surface brightness distribution of the galaxy. Since the fitting algorithm is based on the χ^2 minimization, it is important to start the procedure

TABLE 1
WINGS BCGs SAMPLE

Name	α (J2000) hh:mm:ss	δ (J2000) dd:mm:ss	L_x 10^{44} erg/s	z
A85	00:41:50.45	-09:18:11.5	4.28	0.0551
A119	00:56:16.12	-01:15:19.0	1.65	0.0444
A133	01:02:41.72	-21:52:55.4	1.82	0.0566
A147	01:08:12.04	+02:11:38.2	0.28	0.0447
A151	01:08:51.13	-15:24:23.0	0.52	0.0532
A160	01:12:59.57	+15:29:28.8	0.19	0.0438
A168	01:14:57.58	+00:25:51.1	0.56	0.0450
A193	01:25:07.64	+08:41:57.2	0.79	0.0485
A311	02:09:28.41	+19:46:36.2	0.41	0.0661
A376	02:46:03.94	+36:54:19.1	0.71	0.0476
A500	04:38:52.51	-22:06:39.0	0.72	0.0678
A548b	05:45:29.62	-25:55:56.8	0.15	0.0416
A602	07:53:26.61	+29:21:34.4	0.57	0.0619
A671	08:28:31.66	+30:25:53.0	0.45	0.0507
A754	09:08:32.39	-09:37:47.3	4.09	0.0547
A780	09:18:05.68	-12:05:43.2	3.38	0.0539
A957	10:13:38.27	-00:55:31.2	0.40	0.0451
A970	10:17:25.71	-10:41:20.2	0.77	0.0591
A1069	10:39:43.44	-08:41:12.3	0.48	0.0653
A1291	11:32:23.22	+55:58:03.0	0.22	0.0509
A1631a	12:53:18.41	-15:32:03.8	0.37	0.0461
A1644	12:57:11.60	-17:24:34.0	0.04	0.0467
A1668	13:03:46.60	+19:16:17.4	0.81	0.0634
A1736	13:26:44.09	-27:26:21.8	1.21	0.0458
A1795	13:48:52.51	+26:35:34.5	5.67	0.0633
A1831	13:59:15.11	+27:58:34.5	0.97	0.0634
A1983	14:52:55.33	+16:42:10.5	0.24	0.0447
A1991	14:54:31.50	+18:38:32.8	0.69	0.0584
A2107	15:39:38.92	+21:46:58.1	0.56	0.0410
A2124	15:44:59.02	+36:06:33.9	0.69	0.0666
A2149	16:01:28.11	+53:56:50.3	0.42	0.0679
A2169	16:13:58.09	+49:11:22.3	0.23	0.0578
A2256	17:04:27.22	+78:38:25.4	3.60	0.0581
A2271	17:18:16.66	+78:01:06.2	0.32	0.0576
A2382	21:51:55.62	-15:42:21.2	0.46	0.0641
A2399	21:57:01.72	-07:50:22.0	0.51	0.0578
A2415	22:05:26.12	-05:44:31.1	0.86	0.0575
A2457	22:35:40.81	+01:29:05.8	0.73	0.0584
A2572a	23:17:11.95	+18:42:04.7	0.52	0.0390
A2589	23:23:57.44	+16:46:38.3	0.95	0.0419
A2593	23:24:20.08	+14:38:49.8	0.59	0.0417
A2622	23:35:01.47	+27:22:20.9	0.55	0.0610
A2626	23:36:30.49	+21:08:47.3	0.99	0.0548
A2657	23:44:57.42	+09:11:35.2	0.82	0.0402
A2665	23:50:50.55	+06:08:58.9	0.97	0.0556
A2717	00:03:12.95	-35:56:13.3	0.52	0.0490
A2734	00:11:21.64	-28:51:15.5	1.30	0.0625
A3128	03:29:50.60	-52:34:46.8	2.71	0.0600
A3158	03:43:29.69	-53:41:31.7	2.71	0.0593
A3266	04:31:13.27	-61:27:11.9	3.14	0.0593
A3376	06:00:41.09	-40:02:40.4	1.27	0.0461
A3395	06:27:36.25	-54:26:57.9	1.43	0.0500
A3490	11:45:20.15	-34:25:59.3	0.88	0.0688
A3497	11:59:46.30	-31:31:41.6	0.74	0.0680
A3528a	12:54:41.01	-29:13:39.5	0.68	0.0535
A3528b	12:54:22.23	-29:00:46.8	1.01	0.0535
A3530	12:55:35.99	-30:20:51.3	0.44	0.0537
A3532	12:57:21.97	-30:21:49.1	1.44	0.0554
A3556	13:24:06.71	-31:40:11.6	0.48	0.0479
A3558	13:27:56.84	-31:29:43.9	3.20	0.0480
A3560	13:32:25.76	-33:08:08.9	0.67	0.0489
A3667	20:12:27.32	-56:49:36.3	4.47	0.0556
A3716	20:51:56.94	-52:37:46.8	0.52	0.0462
A3809	21:46:59.07	-43:53:56.2	1.15	0.0627
A3880	22:27:54.43	-30:34:31.8	0.95	0.0584
A4059	23:57:00.71	-34:45:32.8	1.58	0.0475
IZW108	21:13:55.90	+02:33:55.4	1.12	0.0483
MKW3s	15:21:51.84	+07:42:32.1	1.37	0.0444
RXJ0058	00:58:22.88	+26:51:52.6	0.22	0.0484
RXJ1022	10:22:37.40	+38:34:45.0	0.18	0.0548
RXJ1740	17:40:32.06	+35:38:46.1	0.26	0.0441
ZwCl1261	07:16:41.24	+53:23:09.4	0.41	0.0644
ZwCl2844	10:02:36.54	+32:42:24.3	0.29	0.0503
ZwCl8338	18:11:05.18	+49:54:33.7	0.40	0.0494
ZwCl8852	23:10:42.27	+07:34:03.7	0.48	0.0408

NOTE. — The X-ray luminosity is shown in the 0.1–2.4 keV ROSAT RASS bandpass and it has been extracted from Ebeling et al. (1996). The redshift information was taken from Cava et al. (2009)

TABLE 2
ACS BCGs SAMPLE

Name	α (J2000) hh:mm:ss	δ (J2000) dd:mm:ss	L_x 10^{44} erg/s	z
RXJ0056.9-2740	00:56:56.1	-27:40:12	1.32	0.563
RXJ0110.3+1938	01:10:18.0	19:38:23	0.55	0.317
RXJ0154.2-5937	01:54:14.8	-59:37:48	1.25	0.360
RXJ0522.2-3625	05:22:14.2	-36:25:04	2.49	0.472
RXJ0826.1+2625	08:26:06.4	26:25:47	0.91	0.351
RXJ0841.1+6422	08:41:07.4	64:22:43	2.24	0.342
RXJ0847.1+3449	08:47:11.3	34:49:16	2.24	0.560
RXJ0926.6+1242	09:26:36.6	12:42:56	2.41	0.489
RXJ0957.8+6534	09:57:53.2	65:34:30	1.60	0.530
RXJ1015.1+4931	10:15:08.5	49:31:32	1.04	0.383
RXJ1117.2+1744	11:17:12.0	17:44:24	0.77	0.305
RXJ1123.1+1409	11:23:10.2	14:09:44	1.40	0.340
RXJ1354.2-0221	13:54:16.9	-02:21:47	2.52	0.546
RXJ1540.8+1445	15:40:53.3	14:45:34	0.96	0.441
RXJ1642.6+3935	16:42:38.9	39:35:53	0.86	0.355
RXJ2059.9-4245	20:59:55.2	-42:45:33	0.81	0.323
RXJ2108.8-0516	21:08:51.2	-05:16:49	0.81	0.319
RXJ2139.9-4305	21:39:58.5	-43:05:14	0.79	0.376
RXJ2202.7-1902	22:02:44.9	-19:02:10	0.82	0.438
RXJ2328.8+1453	23:28:49.9	14:53:12	1.16	0.497

NOTE. — The X-ray luminosity is in the 0.520 keV energy band. Both X-ray luminosity and redshifts have been extracted from Mullis et al. (2003) and references herein.

adopting initial trials for the free parameters as close as possible to their actual values. These initial conditions were obtained by fitting the one-dimensional surface brightness ellipticity and position angle isophotal profiles of the galaxy. The routine works out the best initial conditions by fitting an exponential law at large radii and a bulge (usually Sérsic or de Vaucouleur) model to the residual surface brightness profile that results at subtracting the outer fit component to the overall profile. This ensures that the iteration procedure does not just stop on a local minimum of the χ^2 distribution. In addition, during each iteration of the fitting algorithm the seeing effects were taken into account by convolving the model image with a Moffat point spread function (PSF) with the fast Fourier transform algorithm. The PSF FWHM matches the one measured from the foreground stars in the field. The code also allows to introduce a Gaussian or a star image to reproduce the PSF.

It has been a wide discussion in the literature about the optimum number of components to fit the surface brightness of a BCG. A number of works (Caon, Capaccioli & D’Onofrio 1993; Graham et al. 1996; Patel et al. 2006) argued that a much better model to fit the surface brightness of the BCG comes from a Sérsic profile rather than a de Vaucouleurs profile, since the universality of the latter is uncertain. However, many recent works have shown evidence that the BCG outermost regions can not be described by a Sérsic model and to provide a satisfactory fit, it is necessary the introduction of at least two components (Nelson et al. 2002; Gonzalez et al. 2003, 2005; Seigar, Graham & Jerjen 2007; Liu et al. 2008).

Motivated by the fact that at least two components are necessary to fit the main BCG population, we have decided to fit the whole population of BCGs with two Sérsic+Exponential compo-

nents (D’Onofrio 2001; Seigar, Graham & Jerjen 2007; Vikram et al. 2009). Then, we will call effective radius the effective radius obtained from the Sérsic component. Even if this value does not correspond exactly with the effective radius of the whole galaxy, we have studied the model dependence of the results (see section 6.1) and we have found the results to be robust.

In Figures 2 and 3, we show some examples of the one-dimensional surface brightness of the BCGs in both samples together with the overlapped fits of the Sérsic and Exponential model (solid line), Sérsic model (dashed line) and De Vaucouleur model (dotted line). All the fits have been performed up to 25 mag arcsec⁻² in the V band. We list the results for each sample of the Sérsic+Exponential, Sérsic and De Vaucouleur fits in Appendix A, B and C respectively. Note that the Sérsic+Exponential fits get the best χ^2 values compared to the single component fits.

The sample of five BCGs analyzed in Seigar, Graham & Jerjen (2007) is much deeper than our two BCG samples. They have a surface brightness limit of 27.5-28 for their sample, while we arrive down to $\mu_V=25$. Our objective in this paper is to compare the ‘sizes’ and ‘concentration’ of two different BCGs samples. We have ensured that the results in both samples are consistent, since the resolution for both samples is similar and we arrive up to the same surface brightness limit and use the same procedure.

4. STRUCTURAL PARAMETERS

In this section, we only have considered the BCGs from the WINGS sample with $5 \times 10^{43} < L_x < 2.52 \times 10^{44} \text{ erg s}^{-1}$ in order to match the same X-ray luminosity range as the ACS cluster sample. We have analyzed the structural parameters extracted from the surface brightness analysis for the BCGs for the WINGS and the ACS samples.

4.1. Sizes and shapes

In Figure 4, we show the relation between the Sérsic parameter (n) and the effective radius (r_e) for the BCGs from the WINGS (black points) and the ACS (diamonds) samples. In both cases, we see a trend in the sense that larger BCGs have larger Sérsic parameter. This relation has also been observed for bright elliptical galaxies in nearby galaxy clusters (Caon, Capaccioli & D’Onofrio 1993; Graham & Guzmán 2003; Aguerri et al. 2004). The triangle and the square in Figure 4 show the median values of $\log(n)$ and $\log(r_e)$ for the BCGs from the WINGS and the ACS samples, respectively. The linear fits of these relations are given by:

$$\log n = (0.144 \pm 0.018) + (0.347 \pm 0.018) \log r_e \quad (2)$$

$$\log n = (0.126 \pm 0.018) + (0.389 \pm 0.031) \log r_e \quad (3)$$

for the WINGS and the ACS samples, respectively. These fits have been obtained by using a 3σ clipping algorithm. They are also overplotted in Figure 4 with solid (WINGS) and dotted (ACS) lines. Notice that the slopes are similar within the errors.

In Table 3, we show the median values for the shape parameters, effective radius and mean surface brightness

TABLE 3
SHAPES AND SIZES FOR BCGS SAMPLES

	WINGS($z \sim 0$)	ACS($z \sim 0.5$)
$\langle n \rangle$	2.64 ± 0.12	2.51 ± 0.32
$\langle r_e(\text{kpc}) \rangle$	6.92 ± 1.40	3.35 ± 0.77
$\langle \mu_e(\text{mag/arcsec}^2) \rangle$	20.29 ± 0.23	20.96 ± 0.26

for both samples. The errors have been estimated with a bootstrap algorithm. While both samples have very similar values of the Sérsic parameter ($n(z=0)/n(z \sim 0.5) = 1.05 \pm 0.14$), we do see a difference for the effective radius between both samples. Thus, nearby BCGs are larger than intermediate redshift ones, being $r_e(z=0)/r_e(z \sim 0.5) = 2.06 \pm 0.63$. We have performed a KS test resulting that the galaxy sizes distributions of the nearby and intermediate redshift samples are statistically different. In contrast, the Sérsic parameter distributions of both galaxy samples are not statistically different. The fact that the Sérsic parameter of the BCGs has not changed indicates that the central light concentrations of the BCGs are similar in both samples.

4.2. Kormendy relation

We have also fitted the Kormendy relation (Kormendy 1977) for both samples as shown in Figure 5. In this relation, $\langle \mu_e \rangle$ refers to the median effective surface brightness within r_e . The linear fits are given by:

$$\langle \mu_e \rangle = (16.675 \pm 0.184) + (4.154 \pm 0.209) \log r_e \quad (4)$$

$$\langle \mu_e \rangle = (18.332 \pm 0.161) + (3.346 \pm 0.253) \log r_e \quad (5)$$

for the WINGS and the ACS samples, respectively. These fits have also been performed with a 3σ clipping algorithm. We have obtained a different Kormendy relation for the different samples with a much steeper slope for the local sample. The median values (see Table 3) show that the intermediate redshift BCGs are smaller and have similar effective surface brightness than low redshift ones. Indeed, the KS test show that the mean surface brightness distributions are not statistically different for the WINGS and ACS samples. Our relations agree with the (Bildfell et al. 2008). They recently found a steeper slope (~ 3.96) for the Kormendy relation for BCGs at $0.15 \leq z \leq 0.55$ compared with local ellipticals.

4.3. Structural parameters versus luminosity

In Figure 6, we show the relation between absolute V rest-frame magnitude (M_V) of the fitted Sérsic component and the mean surface brightness, Sérsic parameter and effective radius of the BCGs. For a given luminosity, nearby BCGs have fainter $\langle \mu_e \rangle$, larger r_e and similar Sérsic parameter than the intermediate redshift BCGs sample as it is shown in Table 3.

Notice also the same behavior in the two BCGs samples. Thus, brighter BCGs are larger (the Spearman test provides a significance level of 6.81 and 3.56 σ for the WINGS and the ACS sample respectively), having the

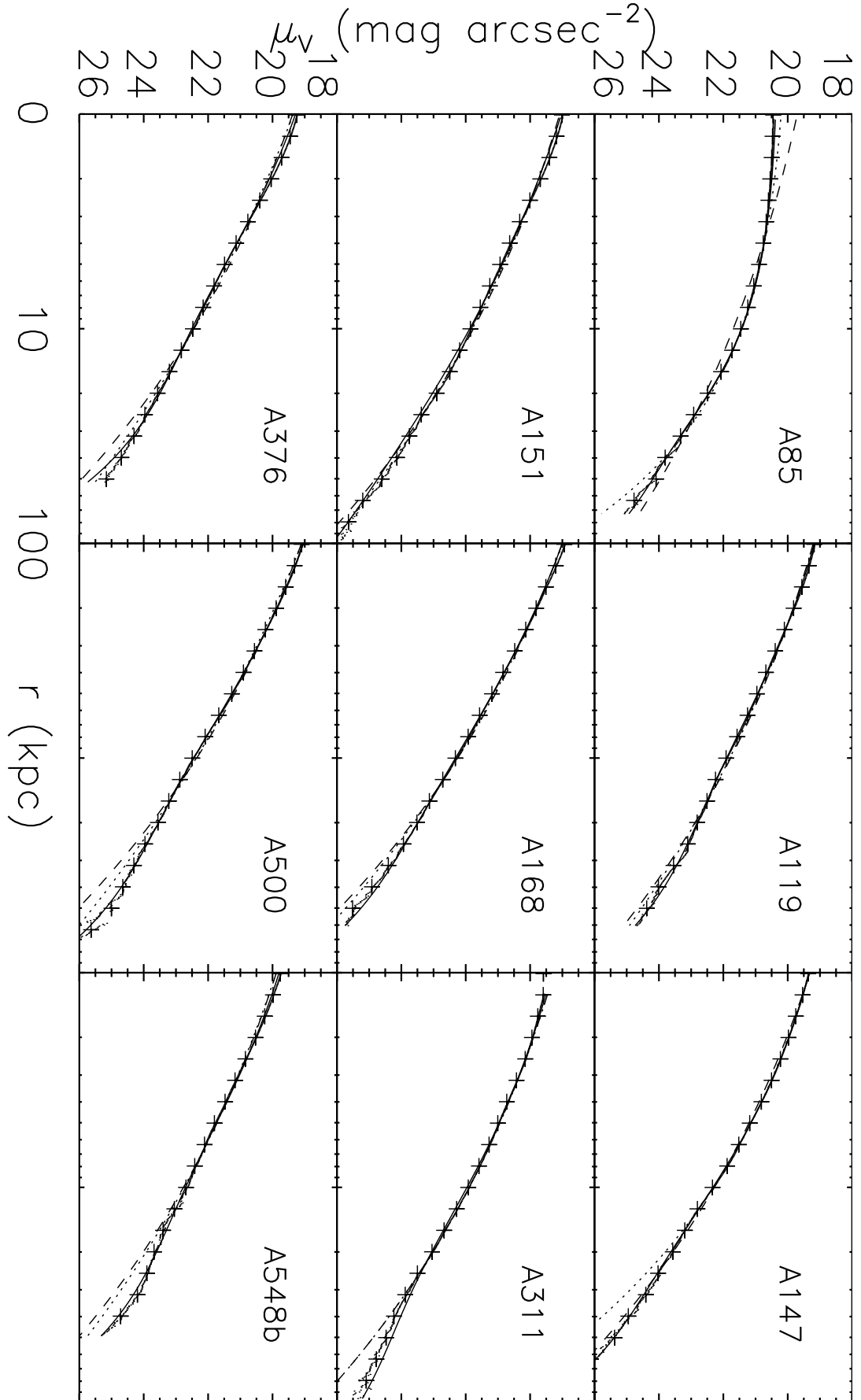


FIG. 2.— One dimensional surface brightness profiles for the first nine BCGs in the WINGS sample (crosses). We overplot the two component Sérsic+Disc fit (solid line), the single Sérsic fit (dashed line) and the single De Vaucouleur fit (dotted line). The axis scale is the same for all the plots.

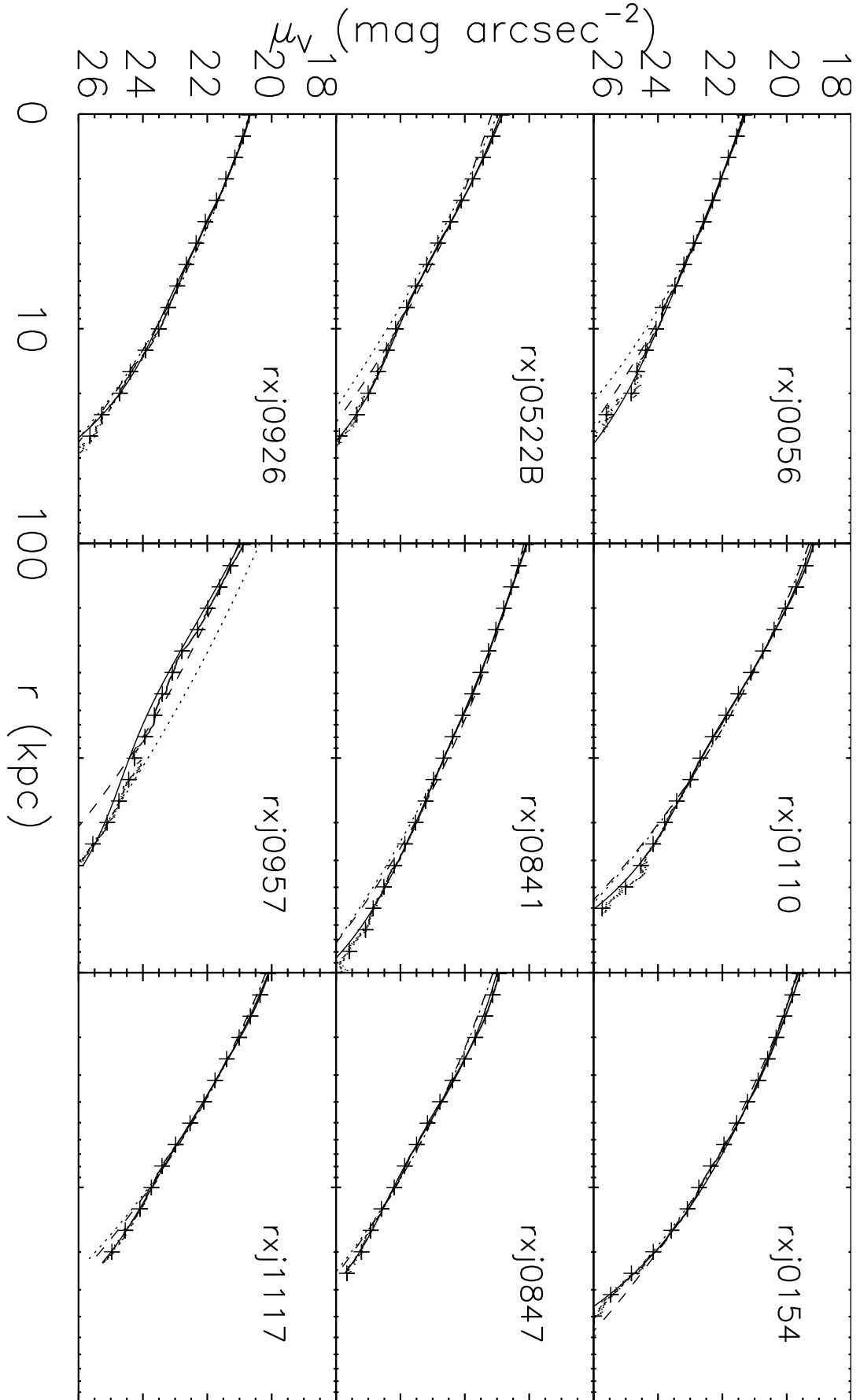


FIG. 3.— One dimensional surface brightness profiles for the first nine BCGs in the ACS sample (crosses). We overplot the two component Sérsic+Disc fit (solid line), the single Sérsic fit (dashed line) and the single De Vaucouleur fit (dotted line). The axis scale is the same for all the plots.

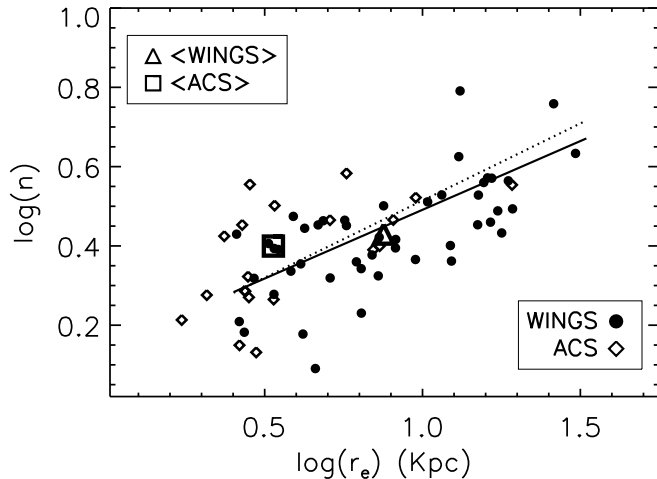


FIG. 4.— Relationship between $\log(r_e) - \log(n)$ for the BCGs in WINGS (black points) and ACS (diamonds). The solid and dotted lines show the fits to the WINGS and ACS samples respectively. The triangle and square show the median value for the WINGS and ACS sample respectively.

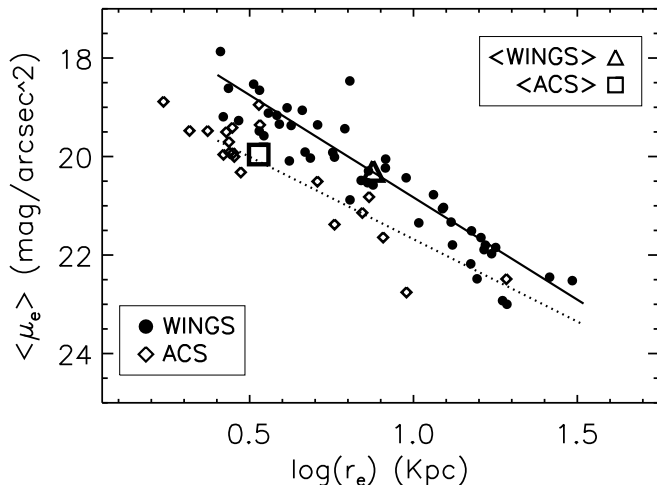


FIG. 5.— Kormendy relation for the BCGs in WINGS (black points) and ACS (diamonds). The solid and dotted lines show the fits to the WINGS and ACS samples respectively. The triangle and square show the median value for the WINGS and ACS samples respectively.

lower redshift sample a steeper slope with respect to the intermediate redshift sample. The linear fits are given by:

$$\log r_e = (-6.966 \pm 0.323) + (-0.356 \pm 0.015)M_V \quad (6)$$

$$\log r_e = (-5.057 \pm 0.316) + (-0.260 \pm 0.015)M_V \quad (7)$$

for the WINGS and ACS sample respectively. The slopes of the local sample agrees with other works (Bernardi et al. 2007).

This size-luminosity relation have also been supported for early-type galaxies by Caon, Capaccioli & D’Onofrio (1993); Gutiérrez et al. (2004); Aguerri et al. (2005a); Liu et al. (2008); Bernardi (2009). BCGs in low redshift clusters have also a significant correlation between absolute magnitude and shape parameter (3.65σ significance in the Spearman test) and between absolute magnitude

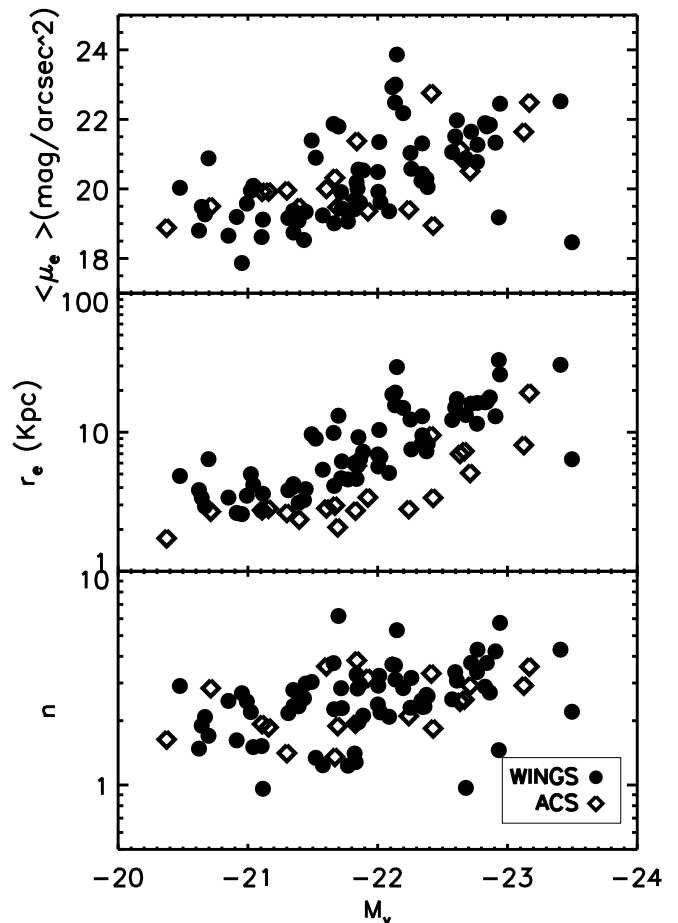


FIG. 6.— Absolute magnitude versus medium surface brightness, Sérsic parameter and effective radius for the BCGs in WINGS (black points) and ACS (diamonds) for the Sérsic component from the two components model fit.

and mean effective surface brightness (4.79σ significance in the Spearman test). However, these tendencies are less significant for the intermediate redshift sample.

5. RELATIONSHIP BETWEEN BCGS AND THEIR HOST CLUSTER.

We have investigated any relationship between the global parameters of the host cluster and the structural parameters of the BCGs. Since most of the information about the host cluster for the ACS sample is not available, we have only considered the WINGS sample. These relations will help to constrain theories of formation and evolution of the clusters and the BCGs themselves. We have considered three different global parameters for the clusters: X-ray cluster luminosity (L_x), the degree of dominance (Δm ; Kim et al. 2002), and the distance between the X-ray peak and the BCG center (D). These parameters indicate different global properties of galaxy clusters.

It is well known that the X-ray cluster luminosity correlates with the temperature of the hot gas present in galaxy clusters (Vikhlinin et al. 2005) and that there is a physical relation between hot gas temperature and mass of the galaxy cluster (Finoguenov et al. 2001; Vikhlinin et al. 2006). Therefore, L_x is an indication of the mass of the cluster (Reiprich & Bohringer 2002).

The degree of dominance is defined as the difference

TABLE 4
SIGNIFICANCE OF THE SPEARMAN TEST FOR THE THE STRUCTURAL
PARAMETERS OF THE BCGS AND THEIR HOST CLUSTER PROPERTIES
IN WINGS SAMPLE.

	$\log L_x$	$\log \Delta m$	$\log D$
$\log n$	0.66	-0.27	0.89
$\log r_e$	-0.49	-2.26	2.32
mag	2.22	3.48	-1.53
$\log B/T$	2.27	1.41	0.06

between the magnitude of the BCG and the mean magnitude of the second and third brightest galaxies of the cluster within the central 500 kpc. It is an indicator of how dominant the BCG is with respect to the cluster. In the hierarchical scenario, the natural evolution of galaxy clusters is to accrete mass to the center of the cluster where the BCGs are located. In other words, clusters with larger Δm would be more evolved systems. The extreme cases are the galaxy fossil clusters or groups (Ponman et al. 1994).

On the other hand, a good indicator of the dynamical state of the galaxy cluster is the closeness of the X-ray center of the cluster and the position of the BCG (Collins et al. 2003; Shan et al. 2010).

In Table 4, we list the significance of the Spearman correlation test for the different relations and in Figure 7, we show the different relationships for the WINGS BCG sample. We find significant correlations between the cluster X-ray luminosity and the BCGs absolute magnitude and the B/T parameter. Thus, more luminous X-ray clusters host BCG with smaller values of B/T, showing that as the cluster becomes more massive, the luminosity of the internal regions of the BCG contributes less to their total light. One possible interpretation is that brighter envelopes are located in BCGs placed in the most X-ray luminous clusters. This behavior is in agreement with previous works (van Dokkum et al. 2010; Liu et al. 2009). In addition, there is a significant tendency of finding more luminous BCGs in more X-ray luminous clusters, consistent with optical-X-ray luminous function (Lin & Mohr 2004; Popesso et al. 2006). If we assume that light trace mass (Reyes et al. 2008), this would imply that BCGs are also more massive in more X-ray luminous clusters as observed in other works, (Burke et al. 2000; Stott et al. 2008).

On the other hand, we do not find a significant correlation between Δm and shape parameter. In contrast, significant correlations are found between Δm and magnitude and effective radius. Thus, BCGs located in clusters with larger degree of dominance are larger and more luminous. These results are in agreement with Bildfell et al. 2008; Niederste-Ostholt et al. 2010 and Smith et al. 2010. The larger and brighter BCGs in massive clusters suggest the evolutionary processes implied in transforming the BCGs are also transforming their host clusters.

The significance of the correlations between the structural parameters and the distance to the center of the cluster are shown in the last column in Table 4. We do see a significant correlation between the location of the BCG in the cluster and the effective radius of the BCG. Thus, larger galaxies tend to be closer to the cen-

ter of the cluster potential well given by X-ray data displaying a more dynamically evolved stage in the cluster. This result agrees with the results obtained from a X-ray analysis of an intermediate redshift cluster sample by Sanderson et al. (2009).

As a conclusion, the properties of the BCGs and their host galaxy clusters are closely related. In particular, larger and brighter BCGs, with smaller B/T are located near to the center of the potential well of very luminous and dominant clusters. This points to a connection between the BCG formation processes and the mass assembly in galaxy clusters. Dynamically evolved and massive galaxy clusters are hosting more massive BCGs, with larger halos, suggesting that the processes happening in the cluster are more active in denser environments.

6. DISCUSSION AND CONCLUSIONS

In the present work, we have performed an analysis of two BCG samples at different redshift ranges. On one hand, we have analyzed the evolution of their structural parameters and on the other, the relation between BCGs and their host galaxy cluster for the WINGS sample. We discuss here the robustness of the results and their implications on the formation and evolution of these particular galaxies.

6.1. Robustness of the results

We have fitted the surface brightness distribution of BCGs with a two components model: Sérsic plus exponential. We have observed that the median values of the structural parameters of the Sérsic fitted component have evolved during the last 6 Gyr. In particular, the effective radius has changed by $r_e(z \sim 0)/r_e(z \sim 0.5) = 2.06 \pm 0.63$. In contrast, the shape Sérsic parameter does not change, being $n(z \sim 0)/n(z \sim 0.5) = 1.05 \pm 0.14$. But, how does these results depend on the fitted model? In order to answer to this question, we have also fitted the surface brightness distribution of our galaxies with a single Sérsic and de Vaucouleurs profiles.

Independent of the fitted model, there is not variation within the last 6 Gyrs in the Sérsic shape parameter. In the case of a single Sérsic fit we have obtained $n(z \sim 0)/n(z \sim 0.5) = 1.02 \pm 0.21$. In contrast, the rate of variation in the size depends on the fitted model. Thus, the change of r_e , when only one single Sérsic component was fitted, becomes by $r_e(z \sim 0)/r_e(z \sim 0.5) = 1.89 \pm 0.36$ and for a single de Vaucouleur fit, we find $r_e(z \sim 0)/r_e(z \sim 0.5) = 1.47 \pm 0.23$. This implies that the growth size rate of the galaxies is smaller when only one component was fitted. However, one single component fits (Sérsic and de Vaucouleurs) give much worse χ^2 values than a Sérsic+ Exponential.

From a model independent perspective, we have measured the size of the galaxies in a different way. We have calculated the 'global' effective radius of BCGs by solving the equation: $L(< r_e) = L_{total}/2$, being L_{total} the total integrated luminosity of the galaxy. In this case, we have obtained that $r_e(z \sim 0)/r_e(z \sim 0.5) = 1.70 \pm 0.15$.

Thus, the effective radius growth extracted from a model independent measurement is smaller but consistent with the growth obtained by using a two component fitting model or a single Sérsic model. Thus, BCGs at $z \sim 0.5$ are smaller than nearby ones with independence of the procedure we use to calculate the sizes.

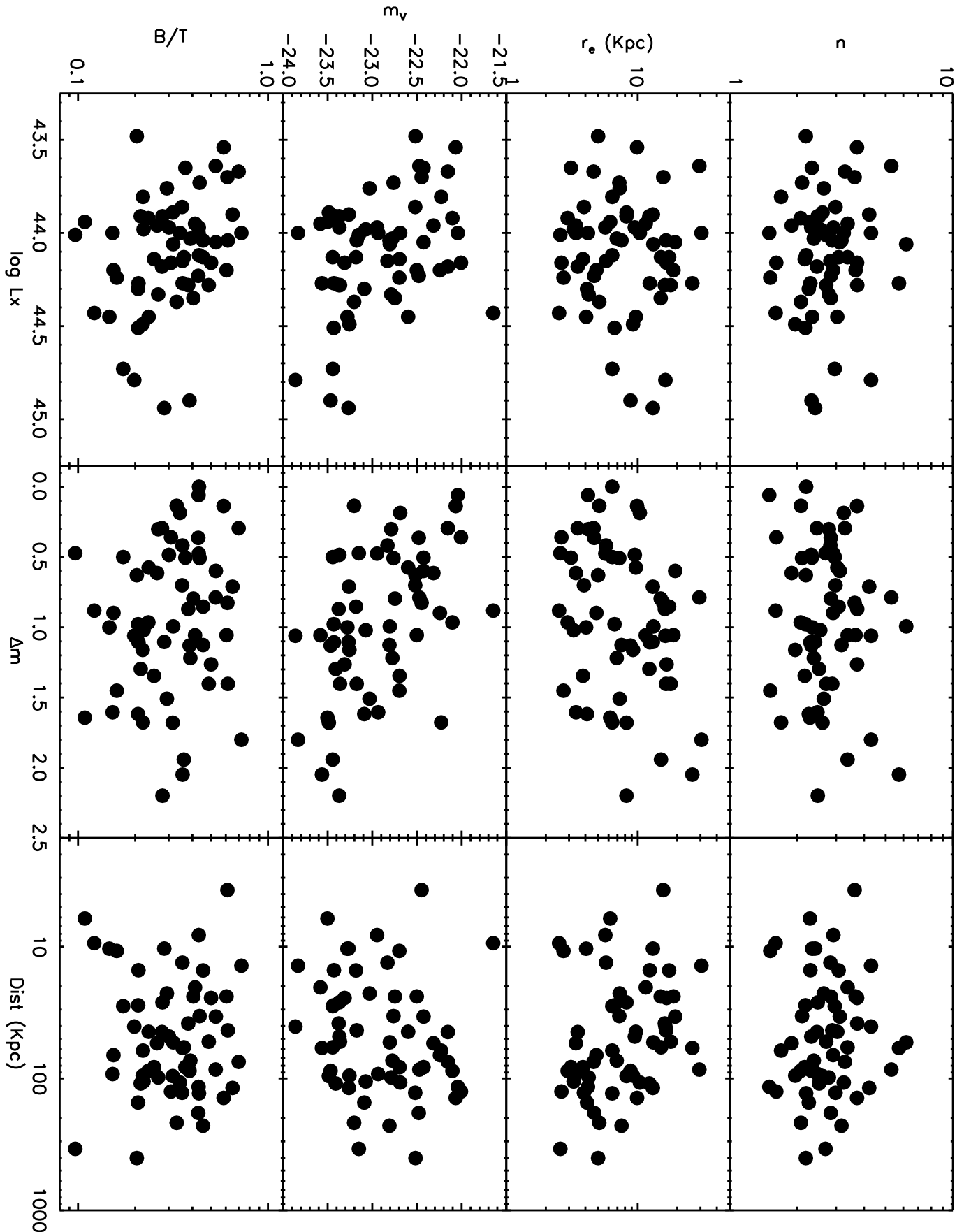


FIG. 7.— Structural parameters of the BCGs (shape parameter, effective radius, ellipticity, absolute magnitude and bulge-to-total light fraction) versus different properties of the host clusters (L_x , degree of dominance and distance from the X-ray center) for the BCGs in WINGS sample.

6.2. Evolution of BCGs during the last 6 Gyrs

There are several observational pieces of evidence about the fact that massive early-type galaxies have grown in size from $z \sim 2$ (Daddi et al. 2005; Trujillo et al. 2006, 2007; van Dokkum et al. 2010). However, Mancini et al. (2010) have presented discrepant results by showing that some high redshift massive elliptical have similar sizes to local ones. As long as BCGs are concerned, Nelson et al. (2002) and Bernardi (2009) reported an increase in the sizes of BCGs at intermediate redshift compared with local ones. Nelson et al. (2002) informed on a factor of ~ 1.7 since $z \sim 0.25$ while Bernardi (2009) published a factor of ~ 2 since $z \sim 0.5$.

Recently, it has been discovered that the Sérsic shape parameters of early-type galaxies has also evolved during the last Gyrs, being larger for nearby galaxies (Vikram et al. 2009; van Dokkum et al. 2010). Indeed, although the mass of massive early-type galaxies has grown from $z \sim 2$ until today, this mass growth has been focused on their external regions (van Dokkum et al. 2010). These results have been interpreted as an inside-out growth of the early-type galaxies, assembling their extended haloes in the last Gyrs. There are several numerical simulations supporting those observed changes of the structural parameters of early-type galaxies. Thus, major or minor mergers produce a growth of the effective radius and Sérsic parameter of the galaxy (Aguerri, Balcells & Peletier 2001; Scannapieco & Tissera 2003; Eliche-Moral et al. 2006; Hopkins et al. 2010).

The results presented in this work show that BCGs have grown in size within the last 6 Gyrs by a factor of ~ 2 . In addition, the growth rate is similar making use of a model independent measurement such as the 'global' effective radius calculated from the whole luminosity. The difference between the evolution of the BCGs and other massive early-type galaxies is the constancy of the Sérsic shape parameter in BCGs since $z \sim 0.6$. The fact that intermediate redshift and nearby BCGs show no evolution in the Sérsic parameter implies that the evolution of these galaxies in the last 6 Gyrs has not been driven by galaxy mergers because major or minor mergers would have changed the shape of the surface brightness distribution of the galaxies.

Numerical simulations show that the structural parameters of early-type galaxies can change due to several processes. In particular, if a galaxy could lose a fraction of its central mass then the radius of the object will grow, and the system will keep the surface brightness profile shape (Hopkins et al. 2010). This process called adiabatic expansion could explain our observables for BCGs. The loss of the inner material could be due to different reasons. Among others, quasar feedback can produce a loss of a considerable fraction of baryonic matter in the center of galaxies (Fan et al. 2008). Central starburst, produced by cooling flows observed in some BCGs (Fabian, Nulsen & Canizares 1982) can also activate galactic winds and superwinds and eject part of the inner mass in galaxies (Tenorio-Tagle et al. 2005; Silich et al. 2010). Displacement of black holes from galaxy center transfer energy to stars in the nucleus and can convert density cusp profiles in core ones. This would also produce an enlarge of the system (Merritt et al.

2004).

In summary, according to our observations, we conclude that the only mechanisms that are able to explain the BCGs evolution in size but not in shape during the last 6 Gyrs are feedback processes. Thus, the evolution of BCGs within the last 6 Gyrs is driven by feedback processes rather than merger evolution. This result is in contradiction with the results obtained by recent numerical simulations about the origin and evolution of BCGs (De Lucia & Blaizot 2007). These simulations predict an important mass growth of the galaxies via dry mergers in the last 6 Gyrs. Nevertheless, other observational recent works have also observed a small or negligible change of the mass of BCGs in the last 8 Gyrs (Collins et al. 2009; Stott et al. 2010).

We thank the anonymous referee for the valuable comments that improved this paper. We acknowledge Andrea Biviano, Bianca Poggianti and Gianni Fasano for helpful comments. We also thank Alfonso Aragón-Salamanca and Anthony Gonzalez for stimulating and helpful discussion. Special thanks to Dave Wittman. JALA has been founded by the Spanish MICINN under the AYA2010-21887-C04-04 project. BA acknowledges the support of NASA grant NNG05GD32G.

Facilities: INT, HST (ACS), MPG-ESO

APPENDIX

A. RESULTS OF THE 2-COMPONENTS SÉRSIC+EXPONENTIAL FIT

A.1. *WINGS BCGs sample*

Name	μ_e mag/arc sec ²	r_e kpc	e_b	μ_0 mag/arc sec ²	h kpc	e_d	n	PA_b	PA_d	B/T	m_V	χ^2
A85	17.99	13.06	0.80	18.56	35.54	0.57	0.97	53	60	0.30	13.21	2.31
A119	17.63	6.59	0.88	18.02	25.34	0.61	2.19	123	128	0.21	13.04	3.24
A147	17.79	7.25	0.76	19.27	26.56	0.73	2.11	150	137	0.44	13.72	2.20
A151	19.79	29.94	0.80	21.20	68.51	1.00	4.30	163	12	0.72	13.04	0.43
A168	17.95	7.54	0.94	19.02	24.28	0.51	3.17	63	59	0.46	13.69	2.12
A311	18.43	12.23	0.77	19.47	64.55	0.24	2.52	110	122	0.21	13.96	28.39
A376	17.21	3.79	0.93	18.06	15.93	0.81	2.17	6	4	0.25	13.92	2.94
A500	18.29	5.73	0.78	19.55	24.19	0.63	2.83	6	36	0.35	14.59	0.45
A548b	18.70	4.87	0.91	19.17	19.64	0.69	2.19	16	131	0.20	13.80	0.67
A602	20.13	18.93	0.94	20.19	32.77	0.32	3.12	62	72	0.53	14.79	10.06
A671	18.21	11.39	0.80	18.65	30.29	0.63	3.38	115	120	0.41	13.19	5.45
A754	17.70	8.81	0.67	18.29	24.30	0.75	2.33	18	29	0.39	13.47	4.21
A957	17.66	8.05	0.79	18.31	27.49	0.64	2.61	11	152	0.32	13.01	10.21
A970	17.43	3.46	0.93	18.51	15.51	0.68	2.46	23	43	0.28	14.96	2.95
A1069	16.62	3.19	0.74	17.49	15.27	0.74	2.55	180	0	0.22	14.27	13.04
A1291	21.13	29.13	0.81	19.83	30.62	0.32	5.30	168	171	0.53	14.30	5.45
A1631a	17.72	3.84	0.76	18.39	12.50	0.70	2.98	145	148	0.35	14.03	0.67
A1644	18.28	3.82	0.83	18.01	17.77	0.60	1.48	51	42	0.08	13.47	3.61
A1668	20.09	18.36	0.87	18.78	15.12	0.57	3.67	153	167	0.60	14.77	0.90
A1736	17.36	5.20	0.62	18.49	20.34	0.55	2.09	137	132	0.33	13.34	0.71
A1795	17.42	5.88	0.87	18.25	27.97	0.65	1.40	103	101	0.17	13.81	4.75
A1831	19.15	15.78	0.86	18.81	32.24	0.44	3.73	71	59	0.38	13.89	2.64
A1983	17.05	4.62	0.74	18.67	11.51	0.59	3.28	117	119	0.70	14.33	3.25
A1991	19.23	16.99	0.81	18.87	28.01	0.47	3.08	101	98	0.46	13.90	6.89
A2107	18.87	16.26	0.86	19.36	28.30	0.52	2.88	17	33	0.62	13.12	2.62
A2124	19.13	14.77	0.90	18.20	23.37	0.60	3.37	71	52	0.36	13.94	2.56
A2149	17.27	2.92	0.87	19.21	20.99	0.73	2.08	26	35	0.23	15.33	2.83
A2169	16.45	3.10	0.70	19.12	23.20	0.65	2.34	176	174	0.37	14.63	1.46
A2256	17.33	5.91	0.86	17.77	16.69	0.83	1.28	56	27	0.28	13.90	3.21
A2271	18.67	6.40	0.78	18.89	20.78	0.68	1.70	29	34	0.22	14.82	6.25
A2382	18.16	3.42	0.77	18.82	12.41	1.00	1.90	8	180	0.26	14.98	0.35
A2399	17.86	4.13	0.67	18.76	10.81	0.77	1.51	103	110	0.43	15.02	0.36
A2415	17.25	4.62	0.80	18.32	15.26	0.61	2.84	121	114	0.43	14.57	2.62
A2457	18.88	16.26	0.72	20.16	54.68	0.39	3.72	175	173	0.50	13.77	1.10
A2572a	16.74	2.52	0.92	18.06	24.35	0.65	2.69	136	87	0.10	13.03	12.16
A2589	20.10	25.46	0.86	18.67	36.76	0.37	5.74	84	95	0.36	12.78	6.59
A2593	19.79	13.18	0.73	17.23	12.55	0.60	6.18	168	164	0.32	13.53	2.88
A2622	17.82	6.91	0.86	18.42	19.13	0.57	2.38	35	37	0.39	14.40	3.37
A2657	18.48	4.74	0.81	18.12	16.59	0.60	2.91	29	5	0.15	14.01	2.11
A2665	19.05	17.64	0.86	19.78	43.81	0.48	2.71	20	3	0.49	13.61	1.71
A2717	18.22	3.37	0.96	18.92	18.60	1.00	2.47	168	11	0.15	13.76	0.85
A2734	19.25	8.86	0.83	19.40	27.46	0.57	1.34	24	19	0.20	14.30	0.44
A3128	18.09	4.17	0.80	19.03	18.69	0.79	2.78	2	61	0.26	14.36	0.97
A3158	18.69	6.49	0.90	19.37	34.32	0.62	2.96	74	95	0.17	13.68	0.46
A3266	19.96	16.47	0.86	19.60	54.47	0.37	4.30	68	72	0.20	13.26	1.16
A3376	17.27	3.55	0.72	18.33	14.46	0.63	0.96	64	67	0.23	13.96	0.51
A3395	19.53	9.81	0.62	19.10	25.79	0.34	3.04	124	126	0.24	14.13	0.66
A3490	17.34	2.76	0.94	18.14	13.85	0.59	1.52	18	29	0.16	14.76	0.68
A3497	17.43	2.62	0.92	19.01	12.45	0.71	1.62	57	35	0.31	15.42	0.47
A3528a	17.36	4.53	0.76	17.08	8.81	0.95	1.23	96	156	0.30	13.63	4.27
A3528b	17.64	4.07	0.83	18.68	21.39	0.59	2.26	1	176	0.21	13.80	0.98
A3530	18.42	6.17	0.79	18.99	38.25	0.40	2.29	126	136	0.11	13.40	1.43
A3532	17.97	4.00	0.86	19.04	26.39	0.72	2.34	46	90	0.15	13.69	0.42
A3556	17.90	5.77	0.66	18.55	15.67	0.69	2.92	144	163	0.43	13.69	0.82
A3558	18.16	5.47	0.93	18.04	20.21	0.62	1.24	180	159	0.12	13.13	0.88
A3560	16.66	6.35	0.78	17.29	16.03	0.96	2.20	72	92	0.43	12.14	3.48
A3667	19.48	12.89	0.82	19.82	40.30	0.44	2.41	67	146	0.28	13.70	0.91
A3716	19.63	10.22	0.99	19.58	24.97	0.45	3.24	88	58	0.34	13.87	0.61
A3809	20.11	14.85	0.87	21.06	48.80	0.39	2.84	89	84	0.40	14.50	0.26
A3880	19.65	12.30	0.98	20.04	47.74	0.50	2.30	0	153	0.21	13.65	0.45
A4059	19.03	9.27	0.75	18.99	27.51	0.56	1.97	160	158	0.22	13.36	0.36
MKW3s	17.62	2.50	0.97	18.52	15.55	0.55	1.61	6	12	0.12	14.82	2.75
RXJ1022	19.03	9.70	0.80	19.42	18.29	0.51	3.72	164	159	0.58	14.87	2.23
RXJ1740	19.43	15.48	0.74	18.85	17.58	0.39	3.63	109	108	0.61	14.00	1.53
ZwCl1261	17.89	8.19	0.85	18.48	29.34	0.52	2.48	42	50	0.28	13.94	2.52
ZwCl2844	17.51	7.15	0.83	19.31	43.66	0.29	2.64	48	52	0.29	13.72	3.58
ZwCl8338	18.50	13.03	0.82	19.14	24.68	0.59	4.22	89	49	0.65	13.45	3.14
ZwCl8852	17.85	9.40	0.71	18.82	37.38	0.48	2.32	100	111	0.30	12.91	2.51
A3562	17.49	7.86	0.78	18.70	43.30	0.43	1.46	89	81	0.18	12.46	0.83

A.2. ACS BCGs sample

Name	μ_e mag/arc sec ²	r_e kpc	e_b	μ_0 mag/arc sec ²	h kpc	e_d	n	PA_b	PA_d	B/T	m_V	χ^2
rxj0056	18.36	9.52	0.88	17.55	16.99	0.55	3.33	59	21	0.33	18.58	4.51
rxj0110	16.09	3.38	0.93	17.37	14.95	0.75	1.84	135	156	0.29	17.03	7.81
rxj0154	17.25	6.98	0.70	17.09	9.47	0.67	2.46	129	157	0.57	17.69	7.06
rxj0522	16.64	2.82	0.80	17.56	14.35	0.84	1.86	19	120	0.18	18.45	3.92
rxj0841	19.19	19.21	0.74	18.45	35.67	0.41	3.58	18	14	0.33	16.82	4.16
rxj0847	16.11	2.97	0.87	17.07	12.21	0.83	1.35	86	36	0.24	18.67	5.42
rxj0926	16.16	2.63	0.77	16.59	10.32	0.59	1.41	137	137	0.18	18.63	7.42
rxj0957	16.68	2.84	0.94	17.90	19.66	0.75	3.59	0	20	0.18	18.48	8.13
rxj1117	16.87	2.75	0.83	18.05	10.28	0.68	1.93	130	155	0.35	18.44	5.42
rxj1123	16.82	3.40	0.89	17.46	14.61	0.75	3.18	55	107	0.24	17.45	21.13
rxj1354	17.13	8.08	0.79	17.43	18.02	0.78	2.92	116	97	0.45	17.83	8.11
rxj1540	15.96	2.07	0.94	16.85	7.35	0.97	1.89	162	99	0.31	18.48	1.37
rxj1642	16.65	1.73	0.99	17.71	10.81	0.88	1.63	142	77	0.14	18.47	8.30
rxj2059	17.48	2.68	0.89	18.32	14.90	0.89	2.84	70	89	0.18	18.09	5.14
rxj2108	17.57	7.32	0.83	18.64	24.17	0.59	2.51	91	77	0.42	17.23	6.15
rxj2139	16.40	5.09	0.60	17.49	13.34	0.49	2.92	164	170	0.55	17.75	5.12
rxj2202	15.67	2.80	0.82	17.44	13.45	0.89	2.10	33	75	0.37	17.96	6.57
rxj2328	16.09	2.73	0.95	17.39	15.16	0.77	1.94	17	83	0.21	18.28	6.08
rxj0826	16.25	2.36	0.75	17.61	10.56	0.66	2.66	60	61	0.34	18.38	15.85
rxj1015	18.05	5.74	0.86	18.49	17.14	0.60	3.83	113	86	0.37	18.36	4.79

NOTE. Col. (1): Galaxy Cluster; Col. (2): Effective surface brightness of the bulge at r_e ; Col. (3): Effective radius of the bulge; Col. (4): Ellipticity of the bulge; Col. (5): Central surface brightness of the disk; Col. (6): Scale length of the disk; Col. (7): Ellipticity of the disk; Col. (8): Shape parameter of the bulge; Col. (9): Position angle of the bulge; Col. (10): Position angle of the disk; Col. (11): bulge-to-total luminosity ratio; Col. (12): V band rest frame magnitude calculated from the model; Col. (13): χ^2 of the fit

B. RESULTS OF THE 1-COMPONENT SÉRSIC FIT

B.1. WINGS BCGs sample

Name	μ_e mag/arc sec ²	r_e kpc	e_b	n	PA_b	m_V	χ^2
A85	18.63	25.07	0.73	1.51	57	13.39	3.97
A119	20.92	64.93	0.78	4.92	126	12.47	4.85
A147	18.50	11.95	0.76	2.69	148	14.10	4.28
A151	20.61	52.84	0.78	4.97	152	13.00	8.67
A168	19.47	20.14	0.86	4.66	61	13.52	3.13
A311	20.06	36.82	0.68	4.00	115	13.92	29.69
A376	21.25	49.33	0.90	5.99	4	13.30	4.57
A500	21.12	31.48	0.77	5.74	11	14.34	0.78
A548b	21.74	38.02	0.95	4.69	168	13.43	1.15
A602	20.74	31.50	0.87	3.57	67	14.60	10.35
A671	20.68	56.78	0.76	5.60	117	12.77	6.52
A754	20.28	47.61	0.69	4.58	20	13.11	5.39
A957	20.86	59.30	0.81	5.70	0	12.54	7.89
A970	21.37	37.07	0.88	6.70	32	14.44	4.65
A1069	20.45	39.89	0.77	5.30	0	13.83	12.32
A1291	21.05	37.74	0.69	4.50	170	14.24	7.41
A1631a	21.43	38.65	0.74	6.59	146	13.40	0.87
A1644	21.75	77.32	0.68	3.84	45	12.62	3.97
A1668	20.25	28.16	0.79	3.45	161	14.53	2.66
A1736	19.71	23.51	0.60	4.21	136	13.20	1.38
A1795	21.57	94.66	0.74	5.04	99	13.09	97.00
A1831	21.56	81.93	0.77	5.88	64	13.27	3.99
A1983	17.91	7.89	0.72	4.17	118	14.25	3.61
A1991	20.16	39.01	0.72	3.66	99	13.64	7.62
A2107	19.46	26.26	0.81	3.31	23	13.00	2.89
A2124	20.86	62.26	0.80	4.48	58	13.37	4.28
A2149	20.61	16.91	0.87	7.90	29	15.59	10.69
A2169	18.88	11.44	0.69	5.48	175	14.83	4.83
A2256	18.98	20.62	0.86	2.63	42	13.81	5.82
A2271	22.33	79.69	0.75	5.04	32	14.03	4.35
A2382	22.32	50.20	0.87	5.50	10	14.30	0.59
A2399	19.31	10.96	0.69	2.80	104	14.99	0.71
A2415	19.60	19.70	0.75	5.31	118	14.28	3.41
A2457	20.16	36.09	0.70	5.00	174	13.67	1.33
A2572a	21.33	49.27	0.86	6.30	121	12.99	42.62
A2589	21.61	85.79	0.72	6.10	92	12.45	8.63
A2593	20.91	56.56	0.65	5.21	164	12.81	11.15
A2622	19.29	19.87	0.79	3.63	36	14.23	4.00
A2657	21.18	44.40	0.73	4.30	15	13.53	3.41
A2665	19.90	33.05	0.83	3.38	15	13.53	1.93
A2717	21.32	31.30	1.00	4.30	180	13.77	2.78
A2734	20.94	35.89	0.75	2.70	22	14.14	0.50

A3128	20.84	24.47	0.87	4.90	16	14.32	1.81
A3158	22.03	59.79	0.86	5.70	84	13.49	1.04
A3266	21.80	63.21	0.73	5.90	74	13.28	2.32
A3376	19.36	14.66	0.68	2.75	66	13.98	2.01
A3395	21.46	46.49	0.54	4.30	125	13.75	1.01
A3490	21.09	32.11	0.87	5.01	0	14.25	2.07
A3497	19.37	8.77	0.88	3.48	47	15.49	1.28
A3528a	18.44	12.50	0.90	2.09	104	13.55	4.70
A3528b	21.94	51.49	0.77	7.90	180	13.44	2.85
A3530	21.93	71.45	0.70	5.10	133	13.09	2.11
A3532	21.93	39.08	0.95	7.10	36	13.95	4.54
A3556	20.77	34.83	0.67	5.61	147	13.23	1.18
A3558	20.86	52.57	0.77	3.30	161	12.56	1.28
A3560	18.49	19.93	1.00	3.67	126	12.01	7.62
A3667	21.15	39.25	0.93	3.76	88	13.51	1.27
A3716	21.34	33.17	1.00	4.64	0	13.50	1.11
A3809	21.03	28.28	0.83	3.61	87	14.49	0.29
A3880	21.23	41.88	0.90	3.44	159	13.63	0.72
A4059	21.17	51.12	0.68	3.54	159	13.00	0.49
MKW3s	22.35	58.11	0.75	5.90	12	14.09	4.41
RXJ1022	20.23	22.13	0.76	4.78	163	14.62	2.52
RXJ1740	19.05	16.82	0.65	2.90	110	14.02	4.40
ZwCl1261	20.40	44.64	0.77	4.70	46	13.58	3.97
ZwCl2844	18.87	16.87	0.74	4.05	50	13.77	6.44
ZwCl8338	21.12	52.44	0.90	7.90	108	12.97	10.23
ZwCl8852	20.36	47.84	0.66	4.61	104	12.63	3.63
A3562	19.01	23.45	0.70	2.68	85	12.76	1.37

B.2. ACS BCGs sample

Name	μ_e mag/arc sec ²	r_e kpc	e_b	n	PA_b	m_V	χ^2
rxj0056	18.57	13.90	0.90	3.10	59	18.87	3.26
rxj0110	18.70	17.41	0.88	4.25	146	16.88	11.16
rxj0154	17.86	12.36	0.72	2.80	136	17.55	7.91
rxj0522	20.89	34.66	0.90	6.70	12	18.34	4.41
rxj0841	21.08	79.17	0.69	4.90	17	16.36	1.27
rxj0847	18.77	17.11	0.90	3.59	68	18.52	8.50
rxj0926	18.84	19.49	0.66	3.56	137	18.30	8.68
rxj0957	20.38	41.96	0.30	7.50	168	18.84	41.41
rxj1117	18.63	8.61	0.81	3.51	138	18.43	7.80
rxj1123	20.29	25.11	0.96	7.90	72	17.43	11.76
rxj1354	19.14	31.77	0.79	4.61	115	17.49	9.79
rxj1540	19.26	16.52	0.96	4.98	156	18.23	6.10
rxj1642	20.95	22.46	1.00	6.70	0	18.49	9.54
rxj2059	21.42	25.84	0.97	7.70	62	18.36	6.95
rxj2108	18.99	18.86	0.80	3.75	86	17.18	6.96
rxj2139	17.78	12.35	0.58	4.24	165	17.60	5.80
rxj2202	17.39	7.74	0.86	3.70	32	18.27	4.42
rxj2328	19.86	21.15	1.00	7.10	26	18.37	17.98
rxj0826	19.08	11.71	0.76	6.30	60	18.35	14.13
rxj1015	20.95	31.36	0.87	7.30	113	18.07	2.59

NOTE. Col. (1): Galaxy Cluster; Col. (2): Effective surface brightness of the bulge at r_e ; Col. (3): Effective radius of the bulge; Col. (4): Ellipticity of the bulge; Col. (5): Shape parameter of the bulge; Col. (6): Position angle of the bulge; Col. (7): V band rest frame magnitude calculated from the model; Col. (8): χ^2 of the fit

C. RESULTS OF THE 1-COMPONENT DE VAUCOULEUR FIT

C.1. WINGS BCGs sample

Name	μ_e mag/arc sec ²	r_e kpc	e_b	PA_b	m_V	χ^2
A85	21.33	112.55	0.73	57	12.32	20.12
A119	20.09	40.90	0.78	126	12.76	5.46
A147	19.68	22.87	0.77	149	13.66	16.40
A151	19.82	34.24	0.78	151	13.26	9.25
A168	19.02	16.04	0.86	61	13.64	3.54
A311	20.06	36.86	0.68	115	13.92	29.81
A376	19.62	20.01	0.90	3	13.83	7.06
A500	19.82	15.86	0.77	11	14.72	1.13
A548b	21.06	25.47	0.96	168	13.70	1.24
A602	21.15	39.89	0.87	67	14.44	10.50
A671	19.53	30.92	0.76	116	13.11	8.18
A754	19.81	36.97	0.69	20	13.26	5.83
A957	19.58	30.23	0.81	178	12.92	19.73
A970	19.37	12.50	0.91	32	15.04	7.36
A1069	19.77	30.42	0.72	180	13.96	30.53
A1291	20.68	31.30	0.69	169	14.35	8.04

A1631a	19.52	14.08	0.73	146	13.96	2.04
A1644	21.92	86.20	0.68	45	12.54	3.98
A1668	20.67	35.07	0.79	161	14.40	2.88
A1736	19.54	21.47	0.60	136	13.25	1.39
A1795	20.66	57.30	0.74	100	13.39	97.26
A1831	20.02	34.99	0.77	65	13.77	4.83
A1983	17.82	7.55	0.72	118	14.27	3.67
A1991	20.43	45.07	0.72	99	13.56	7.70
A2107	20.00	34.72	0.81	23	12.83	3.40
A2124	20.44	49.50	0.80	58	13.51	4.37
A2149	19.57	12.18	0.84	27	15.66	7.51
A2169	17.95	7.15	0.70	175	15.07	5.72
A2256	20.19	39.28	0.87	42	13.40	12.22
A2271	21.43	48.16	0.75	32	14.34	4.59
A2382	21.03	24.29	0.88	10	14.75	0.87
A2399	20.27	18.14	0.69	104	14.69	1.24
A2415	18.81	13.34	0.76	116	14.48	5.02
A2457	19.40	24.11	0.70	174	13.90	1.75
A2572a	20.37	36.49	0.80	106	13.00	22.63
A2589	20.05	39.70	0.72	92	12.77	21.86
A2593	20.01	34.98	0.65	164	13.08	11.75
A2622	19.59	23.27	0.79	36	14.14	4.15
A2657	20.98	40.62	0.73	12	13.56	4.09
A2665	20.46	45.15	0.83	15	13.33	2.22
A2717	21.12	28.80	0.97	121	13.81	2.91
A2734	22.34	82.28	0.74	21	13.54	0.94
A3128	20.24	18.15	0.87	14	14.48	2.42
A3158	20.65	28.19	0.85	86	13.93	2.05
A3266	20.64	38.31	0.70	72	13.47	3.00
A3376	20.51	27.44	0.68	66	13.59	2.69
A3395	21.23	42.05	0.53	125	13.81	1.12
A3490	20.25	20.21	0.87	0	14.52	2.22
A3497	19.79	10.94	0.88	47	15.36	1.36
A3528a	20.02	25.44	1.00	180	13.13	
A3528b	20.16	23.52	0.74	179	13.76	1.86
A3530	20.93	40.76	0.68	132	13.46	2.79
A3532	20.15	17.52	0.87	40	14.30	2.45
A3556	19.50	17.47	0.68	147	13.63	1.83
A3558	21.61	83.06	0.76	159	12.23	2.33
A3560	18.78	25.60	0.83	73	11.90	4.36
A3667	21.37	44.67	0.93	88	13.43	1.27
A3716	20.78	24.40	1.00	64	13.69	1.16
A3809	21.38	34.45	0.83	87	14.37	0.31
A3880	21.80	58.25	0.90	159	13.41	0.75
A4059	21.62	66.61	0.68	159	12.82	0.53
MKW3s	20.77	24.70	0.74	12	14.59	5.10
RXJ1022	19.74	17.42	0.75	164	14.75	2.88
RXJ1740	19.94	26.02	0.67	109	13.77	3.12
ZwCl1261	19.81	32.21	0.77	46	13.78	4.35
ZwCl2844	18.84	16.57	0.74	50	13.78	6.44
ZwCl8338	18.77	17.30	0.84	79	13.47	6.75
ZwCl8852	19.82	35.50	0.66	104	12.81	3.61
A3562	20.30	48.54	0.69	85	12.28	1.72

C.2. ACS BCGs sample

Name	μ_e mag/arc sec ²	r_e kpc	e_b	PA_b	m_V	χ^2
rxj0056	19.64	28.82	0.85	41	18.27	5.37
rxj0110	18.51	15.75	0.88	146	16.94	11.25
rxj0154	18.79	19.98	0.72	136	17.26	11.51
rxj0522	19.80	23.89	0.92	6	18.31	7.56
rxj0841	20.34	56.45	0.65	16	16.52	5.26
rxj0847	19.14	20.97	0.90	68	18.39	8.64
rxj0926	19.22	23.92	0.66	137	18.17	8.85
rxj0957	18.73	13.10	0.89	0	18.88	18.56
rxj1117	19.03	10.59	0.81	138	18.31	8.21
rxj1123	19.13	18.51	0.89	87	17.38	29.49
rxj1354	18.57	22.88	0.79	116	17.71	9.96
rxj1540	18.44	10.47	0.97	151	18.51	7.53
rxj1642	20.18	20.06	1.00	0	18.24	12.12
rxj2059	20.25	19.13	1.00	48	18.16	11.35
rxj2108	19.19	21.03	0.80	86	17.11	7.03
rxj2139	17.63	11.46	0.58	166	17.64	6.05
rxj2202	17.74	9.58	0.86	36	18.11	12.52
rxj2328	18.73	15.24	0.94	69	18.32	11.03
rxj0826	18.14	8.19	0.72	61	18.47	24.45
rxj1015	19.04	12.85	0.84	103	18.46	8.04

NOTE. Col. (1): Galaxy Cluster; Col. (2): Effective surface brightness of the bulge at r_e ; Col. (3): Effective radius of the bulge; Col. (4): Ellipticity of the bulge; Col. (5): Position angle of the bulge; Col. (6): V band rest frame magnitude calculated from the model; Col. (7): χ^2 of the fit

REFERENCES

- Abadi, M. G., Navarro, J. F., & Steinmetz, M. 2006, *MNRAS*, 365, 747
- Aguerri, J. A. L., Balcells, M., & Peletier, R. F. 2001, *A&A*, 367, 428
- Aguerri, J.A.L., Iglesias-Páramo, J., Vilchez J.M et al., 2004, *ApJ*, 127, 1344
- Aguerri, J. A. L., Iglesias-Páramo, J., Vílchez, J. M. et al., 2005, *AJ*, 130, 475
- Aragón-Salamanca, A., Ellis, R. S., Couch, W. J. et al. 1993, *MNRAS*, 262, 764
- Aragón-Salamanca, A., Baugh, C. M., & Kauffmann, G. 1998, *MNRAS*, 297, 427
- Arnaboldi, M., et al. 2002, *AJ*, 123, 760
- Arnaboldi, M., Gerhard, O., Aguerri, J. A. L. et al. 2004, *ApJ*, 614, L33
- Ascaso, B., Moles, M., Aguerri, J. A. L. et al. 2008, *A&A*, 487, 453
- Ascaso B., 2008, Tesis Doctoral, Universidad de Granada.
- Ascaso, B., Aguerri, J. A. L., Moles, M. et al. 2009, *A&A*, 506, 1071
- Bernardi, M., Hyde, J. B., Sheth, R. K. et al. 2007, *AJ*, 133, 1741
- Bernardi, M. 2009, *MNRAS*, 395, 1491
- Bildfell, C., Hoekstra, H., Babul, A. et al. 2008, *MNRAS*, 389, 1637
- Bower, R. G., Lucey, J. R., & Ellis, R. S. 1992, *MNRAS*, 254, 589
- Burke, D. J., Collins, C. A., & Mann, R. G. 2000, *ApJ*, 532, L105
- Brough, S., Collins, C. A., Burke, D. J. et al. 2002, *MNRAS*, 329, L53
- Caon, N., Capaccioli, M., & D'Onofrio, M. 1993, *MNRAS*, 265, 1013
- Castro-Rodríguez, N., Arnaboldi, M., Aguerri, J. A. L. et al. 2009, *A&A*, 507, 621
- Cava, A., et al. 2009, *A&A*, 495, 707
- Collins, C., Brough, S., Burke, D. et al. 2003, *Ap&SS*, 285, 51
- Collins, C. A., Stott, J. P., Hilton, M. et al. 2009, *Nature*, 458, 603
- Coziol, R., Andernach, H., Caretta, C. A. et al. 2009, *AJ*, 137, 4795
- Daddi, E., Renzini, A., Pirzkal, N., et al. 2005, *ApJ*, 626, 680
- De Lucia, G., & Blaizot, J. 2007, *MNRAS*, 375, 2
- Doherty, M., et al. 2009, *A&A*, 502, 771
- D'Onofrio, M. 2001, *MNRAS*, 326, 1517
- Dubinski, J. 1998, *ApJ*, 502, 141
- Ebeling, H., Voges, W., Bohringer, H. et al. 1996, *MNRAS*, 281, 799
- Eliche-Moral, M. C., Balcells, M., Aguerri, J. A. L. et al. 2006, *A&A*, 457, 91
- Fabian, A. C., Nulsen, P. E. J., & Canizares, C. R. 1982, *MNRAS*, 201, 933
- Fan, L., Lapi, A., De Zotti, G. et al. 2008, *ApJ*, 689, L101
- Fasano, G., Marmo, C., Varela, J, et al. 2006, *A&A*, 445, 805
- Fasano, G., Bettoni, D., Ascaso, B., et al. 2010, *MNRAS*, 294
- Finoguenov, A., Reiprich, T. H., & Bohringer, H. 2001, *A&A*, 368, 749
- Freeman, K.C., 1970, *ApJ*, 160, 811
- Gerhard, O., Arnaboldi, M., Freeman, K. C. et al. 2007, *A&A*, 468, 815
- Gonzalez, A. H., Zabludoff, A. I., & Zaritsky, D. 2003, *Ap&SS*, 285, 67
- Gonzalez, A. H., Zabludoff, A. I., & Zaritsky, D. 2005, *ApJ*, 618, 195
- Graham, A., Lauer, T. R., Colless, M. et al. 1996, *ApJ*, 465, 534
- Graham, A. W., & Guzmán, R. 2003, *AJ*, 125, 2936
- Gunn, J. E., & Oke, J. B. 1975, *ApJ*, 195, 255
- Gutiérrez, C. M., Trujillo, I., Aguerri, J. A. L. et al. 2004, *ApJ*, 602, 664
- Hoessel, J. G., & Schneider, D. P. 1985, *AJ*, 90, 1648
- Hopkins, P. F., Bundy, K., Hernquist, L. et al. 2010, *MNRAS*, 401, 1099
- Humason, M. L., Mayall, N. U., & Sandage, A. R. 1956, *AJ*, 61, 97
- Jones, C., & Forman, W. 1984, *ApJ*, 276, 38
- Kim, R. S. J., Annis, J., Strauss, M. A., et al.. 2002, *Tracing Cosmic Evolution with Galaxy Clusters*, 268, 395
- Kormendy, J. 1977, *ApJ*, 217, 406
- Kormendy, J., Fisher, D. B., Cornell, M. E. et al. 2009, *ApJS*, 182, 216
- Lambas, D. G., Groth, E. J., & Peebles, P. J. E. 1988, *AJ*, 95, 996
- Lauer, T. R., Faber, S. M., Richstone, D. et al. 2007, *ApJ*, 662, 808
- Lin, Y.-T., & Mohr, J. J. 2004, *ApJ*, 617, 879
- Lin, Y.-T., Ostriker, J. P., & Miller, C. J. 2009, arXiv:0904.3098
- Liu, F. S., Xia, X. Y., Mao, S. et al. 2008, *MNRAS*, 385, 23
- Liu, F. S., Mao, S., Deng, Z. G. et al. 2009, *MNRAS*, 396, 2003
- Loh, Y.-S., & Strauss, M. A. 2006, *MNRAS*, 366, 373
- Loubser, S. I., Sánchez-Blázquez, P., Sansom, A. E. et al. 2009, *MNRAS*, 398, 133
- Mancini, C., Daddi, E., Renzini, A. et al. 2010, *MNRAS*, 401, 933
- Matthews, T. A., Morgan, W. W., & Schmidt, M. 1964, *ApJ*, 140, 35
- McGlynn, T. A., & Ostriker, J. P. 1980, *ApJ*, 241, 915
- Méndez-Abreu J., Aguerri J.A.L, Corsini E. M et al., 2008, *A&A*, 478, 353
- Merritt, D. 1985, *ApJ*, 289, 18
- Merritt, D., Piatek, S., Portegies Zwart, S. et al. 2004, *ApJ*, 608, L25
- Miley, G.K., Overzier, R.A.; Zirm, A.W., et al. 2006, *ApJ*, 650, L29
- Moore, B., Katz, N., Lake, G. et al. 1996, *Nature*, 379, 613
- Mullis, C. R., McNamara, B. R., Quintana, H., et al. 2003, *ApJ*, 594, 154
- Murante, G., Giovalli, M., Gerhard, O. et al.. 2007, *MNRAS*, 377, 2
- Nelson, A. E., Simard, L., Zaritsky, D. et al. 2002, *ApJ*, 567, 144
- Niederste-Ostholt, M., Strauss, M. A., Dong, F. et al. 2010, *MNRAS*, 560
- Oemler, A. 1973, *ApJ*, 180, 11
- Oemler, A., Jr. 1976, *ApJ*, 209, 693
- Ostriker, J. P., & Tremaine, S. D. 1975, *ApJ*, 202, L113
- Ostriker, J. P., & Hausman, M. A. 1977, *ApJ*, 217, L125
- Patel, P., Maddox, S., Pearce, F. R. et al. 2006, *MNRAS*, 370, 85
- Poggianti, B. M. 1997, *A&AS*, 122, 399
- Ponman, T. J., Allan, D. J., Jones, L. R., et al. 1994, *Nature*, 369, 462
- Popesso, P., Biviano, A., Böhringer, H. et al., 2006, *A&A*, 445, 29
- Postman, M., & Lauer, T. R. 1995, *ApJ*, 440, 28
- Reiprich, T. H., & Bohringer, H. 2002, *ApJ*, 567, 716
- Reyes, R., Mandelbaum, R., Hirata, C. et al. 2008, *MNRAS*, 390, 1157
- Sandage, A. 1972a, *ApJ*, 173, 485
- Sandage, A. 1972, *ApJ*, 178, 1
- Sanderson, A. J. R., Edge, A. C., & Smith, G. P. 2009, *MNRAS*, 398, 1698
- Scannapieco, C., & Tissera, P. B. 2003, *MNRAS*, 338, 880
- Schombert, J. M. 1986, *ApJS*, 60, 603
- Schombert, J. M. 1987, *ApJS*, 64, 643
- Schombert, J. M. 1988, *ApJ*, 328, 475
- Seigar, M. S., Graham, A. W., & Jerjen, H. 2007, *MNRAS*, 378, 1575
- Sérsic, J.L., 1968, *Atlas de Galaxias Australes (Córdoba: Obs. Astron. Univ. Nac. Córdoba)*
- Shan, H., Qin, B., Fort, B. et al. 2010, *MNRAS*, 406, 1134
- Silich, S., Tenorio-Tagle, G., Muñoz-Tuñón, C. et al. 2010, *ApJ*, 711, 25
- Smith, G. P., Kneib, J.-P., Smail, I. et al. 2005, *MNRAS*, 359, 417
- Smith, G. P.; Khosroshahi, H. G.; Dariush, A., et al. 2010, *MNRAS*, in press

- Stanford, S. A., Eisenhardt, P. R., & Dickinson, M. 1998, *ApJ*, 492, 461
- Stott, J. P., Edge, A. C., Smith, G. P. et al. 2008, *MNRAS*, 384, 1502
- Stott, J. P., Collins, C. A., Sahlh, M., et al. 2010, *ApJ*, 718, 23
- Tenorio-Tagle, G., Silich, S., Rodríguez-González, A. et al. 2005, *ApJ*, 628, L13
- Tremaine, S. D., & Richstone, D. O. 1977, *ApJ*, 212, 311
- Trujillo, I., Graham, A. W., & Caon, N. 2001, *MNRAS*, 326, 869
- Trujillo, I., Förster Schreiber, N. M., Rudnick, G., et al. 2006, *ApJ*, 650, 18
- Trujillo, I., Conselice, C. J., Bundy, K. et al. 2007, *MNRAS*, 382, 109
- van Dokkum, P. G., Franx, M., Kelson, D. D. et al. 1998, *ApJ*, 500, 714
- van Dokkum, P.G., Whitaker, K.E., Brammer, G., et al. 2010, *ApJ*, 709, 1018
- Varela, J., D'Onofrio, M., Marmo, C., et al. 2009, *A&A*, 497, 667
- Vikhlinin, A., Markevitch, M., Murray, S. S. et al. 2005, *ApJ*, 628, 655
- Vikhlinin, A., Kravtsov, A., Forman, W. et al. 2006, *ApJ*, 640, 691
- Vikram, V., Wadadekar, Y., Kembhavi, A. K. et al. 2009, *MNRAS*, L355
- Whiley, I. M.; Aragn-Salamanca, A.; De Lucia, G., et al. 2008, *MNRAS*, 387, 1253
- Zibetti, S., White, S. D. M., Schneider, D. P. et al. 2005, *MNRAS*, 358, 949